ACS Catalysis

Article

Nature of WO Sites on SiO and their Molecular Structure-Reactivity/Selectivity Relationships for Propylene Metathesis

Soe Lwin, Yuanyuan Li, Anatoly I Frenkel, and Israel E. Wachs

ACS Catal., **Just Accepted Manuscript** • DOI: 10.1021/acscatal.6b00389 • Publication Date (Web): 04 Apr 2016

ACS Publications

ACS Catalysis is published by the American Chemical Society. 1155 Sixteenth Street N.W., Washington, DC 20036

Nature of WO_x Sites on SiO_2 and their Molecular Structure-Reactivity/Selectivity Relationships for Propylene Metathesis

Soe Lwin[a], Yuanyuan Li[b], Anatoly I. Frenkel[b], Israel E. Wachs[a*]

[a] *Operando* Molecular Spectroscopy and Catalysis Laboratory, Department of Chemical Engineering, Lehigh University, Bethlehem, PA 18015, USA

[b] Department of Physics, Yeshiva University, New York, NY 10016, USA

*Corresponding author: iew0@lehigh.edu

Abstract

Supported WO_x/SiO_2 catalysts were investigated for propylene metathesis as a function of tungsten oxide loading and temperature. The catalysts were synthesized by incipient-wetness impregnation of an aqueous ammonium metatungstate solution onto the silica support and calcined at elevated temperatures to form the supported tungsten oxide phase. *In situ* Raman spectroscopy under dehydrated conditions revealed that below 8% WO_x/SiO_2, only surface WO_x sites are present on the silica support: dioxo $(O=)_2WO_2$ and mono-oxo $O=WO_4$. The *in situ* XANES analysis showed that dioxo surface WO_4 sites were the dominant surface WO_x sites on SiO_2 (>90%). The isolated nature of the surface WO_x sites was confirmed with *in situ* UV-vis spectroscopy. The surface WO_x sites are activated by exposure to propylene at elevated temperature that removes oxygen from these sites. The activation process produces a highly active surface WO_x site that can perform olefin metathesis at ~150-250°C. For 8% WO_x/SiO_2 and higher tungsten oxide loading, crystalline WO_3 nanoparticles (NPs) are also present and their amount increase with greater tungsten oxide loading but WO_3 NPs, however, are not active for propylene metathesis. The acid character of the surface WO_x sites (Lewis) and WO_3 NPs (Brønsted) are responsible for formation of undesirable reaction products (C_4-C_6 alkanes and dimerization of $C_2^=$ to $C_4^=$). This study represents the *first time* that molecular level structure-activity/selectivity relationships have been established for propylene metathesis by conventionally impregnated supported WO_x/SiO_2 catalysts.

Keywords: catalyst, supported, tungsten oxide, silica, metathesis, propylene; Spectroscopy, in situ, operando, Raman, UV-vis, XAS, TPSR.

1. Introduction

The olefin metathesis reaction was discovered in the early 1960s and became a commercial process in the late 1960s for the production of ethylene and butene from propylene (Phillips Triolefin Process).[1] Nowadays, the reverse process is economically desired due to a world shortage of propylene caused by the shift to lighter feedstocks derived from shale gas fracking.[1] Although homogeneous metathesis catalysts have received much attention, with well-defined model catalysts that exhibit high activity and selectivity, their commercial applications remain quite limited because of issues related to catalyst recovery and product separation.[2] To circumvent these technical issues, the commercial catalyst employed for the Phillips Triolefin Process employs a heterogeneous supported WO_x/SiO_2 catalyst that operates at 400-600°C. The supported WO_x/SiO_2 catalyst consists of a tungsten oxide phase deposited on a high surface area SiO_2 support. The advantages of the supported WO_x/SiO_2 catalyst are (*i*) resiliency to trace quantities of oxygenate in the feed that are poisons for metathesis[2,3], (*ii*) long catalyst lifetime compared to other supported metathesis catalysts based on MoO_x or ReO_x [2], (*iii*) ease of catalyst regeneration to remove deposited coke [3] and (*iv*) absence of catalyst embrittlement upon periodic regeneration.[3] The higher operating temperature of the supported WO_x/SiO_2 catalysts, however, also results in some olefin isomerization and cracking that adversely impact the metathesis selectivity.[4,5]

From early Raman spectroscopy, under ambient conditions where the catalyst is hydrated, and H_2-temperature programmed reduction studies of supported WO_x/SiO_2 catalysts it was proposed that the catalytic active site is a surface compound and not crystalline WO_3 nanoparticles (NPs), but the molecular structure of the surface WO_x compound was not

determined.[6] Van Roosmalen *et al*. initially proposed that the active surface WO_x sites consist of penta-coordinated mono-oxo $O{=}W(OH)_2(\text{-}O\text{-}Si)_2$ and $O{=}W(OH)(\text{-}O\text{-}Si)_3$ coordinated species, but direct evidence for these molecular structures was not provided.[7] Verpoort *et al*. investigated a support consisting of a thin SiO_2 film on a Si(100) single crystal and reacted the silica layer with $C_5H_5W(CO)_3Cl$ in a PhCl solvent to prepare the model catalyst to examine the nature of the deposited WO_x layer after evaporation of the solvent at 120°C with angle resolved-XPS in vacuum.[8-10] The study revealed that the deposited tungsten oxide phase was present as a highly dispersed oxide layer after calcination and it was proposed that the surface tungsten oxide was present as isolated surface WO_4 and polymeric WO_5 sites contained 2 Si-O-W bonds and terminated with either W–OH or W=O functionalities. These model XPS studies, however, can only provide the *average* stoichiometry of the surface tungsten oxide sites and not direct molecular structural information. Basrur *et al*. proposed, without supporting experimental evidence, that dioxo $(O{=})_2W(\text{-}O\text{-}Si)_2$ are the catalytic active sites that become nonstoichiometric upon activation for metathesis.[11] Martin *et al*. performed EXAFS measurements under ambient conditions on supported WO_x/SiO_2 catalysts under ambient conditions and concluded that either hydrated polytungstate chains or Si-containing Keggin-type clusters are present on silica.[12] Several more recent publications about olefin metathesis by supported WO_x/SiO_2 catalysts have been reported, but the characterization studies were also performed under ambient conditions[13-19] where only hydrated polyoxo $(W_{12}O_{39})^{6-}$ clusters and WO_3 NPs are known to be present.[20,21] These studies, however, incorrectly assigned the Raman bands of the hydrated polyoxo tungsten oxide clusters as those belonging to dehydrated surface WO_x sites because of an earlier incorrect assignment by in the literature by Huang *et al.* [19] The molecular and electronic structures of the tungsten oxide phases on silica have been determined by Wachs *et al.* combining *in situ* Raman

and UV-vis spectroscopy.[20-23] Under ambient conditions, hydrated polyoxo $(W_{12}O_{39})^{6-}$ clusters are the dominant surface tungsten oxide species [20,23] and WO_3 nanoparticles (NPs) are also present with increasing tungsten oxide loading. Under dehydrated conditions, the hydrated tungsten oxide polyoxo clusters decompose to isolated surface dioxo, $(O=)_2W(-O)_2$, and mono-oxo $O=W(-O)_4$ species and the WO_3 NPs remain unchanged.[20-23]

In well-defined silica-supported organometallic systems, organic precursors are grafted onto partially dehydroxylated silica (at 200-800°C) and these systems are able to perform metathesis of both linear and functionalized olefins at relatively low temperatures (<100°C).[24-29] Some of the W-organic precursors reported in the recent literature are $[(\equiv Si\text{-}O\text{-})W(=O)Me_3]$,[24] $[W(=O)(=CHtBu)\text{-}(SHMT)_2(PMe_2Ph)]$,[25] $[W(=O)(=CHtBu)(SHMT)_2]$ (SHMT = 2,6-dimesitylthiophenoxide),[25] $(ArO)_2W(=O)(=CHtBu)$ (ArO = 2,6-mesitylphenoxide), [26] $[WOCl_4]$ with $SnMe_4$,[27] $WONp_4$, Np = CH_2-tBu, [28] and $[WO(CH_2SiMe_3)_3Cl]$.[29] These well-defined systems have been characterized with NMR, XANES/EXAFS and IR experiments and DFT calculations. Although their catalytic activity is extremely high, such catalysts cannot be applied in practice to large scale olefin metathesis systems due to their air sensitive nature and inability to regenerate such catalysts. These model silica-supported organometallic catalysts, however, are providing many fundamental insights about the olefin metathesis reaction.

In the present investigation, systematic *in situ* and *operando* UV-vis, XAS (XANES/EXAFS) and Raman spectroscopy under dehydrated and metathesis reaction conditions with transient and steady-state reaction measurements. This is the *first study* to report on the nature of the supported tungsten oxide phase on silica during the olefin metathesis reaction that

allows establishing the molecular structure-activity/selectivity relationships for propylene metathesis by conventionally impregnated supported WO_x/SiO_2 catalysts.

2. Experimental

2.1. Catalyst Synthesis

The SiO_2 support (Cabot, BET surface area= 332 m^2/g) was water treated and dried under ambient conditions overnight before being calcined in air at 500°C for 4 hours. Incipient-wetness impregnation of WO_x is achieved by using ammonium metatungstate hydrate, ($(NH_4)_6H_2W_{12}O_{40} \cdot xH_2O$, Pfaltz and Bauer, 99.5%) in an aqueous solution of water. The samples were initially dried at RT overnight, then at 120°C in air for 2 hours before being calcined in air at 500°C for 4 hours.

2.2. *In situ* UV-vis Spectroscopy

The UV-vis spectra of the catalyst samples were taken using a Varian Cary 5E UV-vis-NIR spectrophotometer with the Harrick Praying Mantis accessory. Approximately 5-25 mg of each catalyst in finely ground powder form was loaded into an *in situ* environmental cell (Harrick, HVC-DR2). Spectra of the dehydrated samples were collected in the 200-800 nm range at 25°C, after the 500°C dehydration, using a scan rate of 15 nm/min and a signal averaging time of 0.6 seconds. A magnesium oxide sample was used as a standard for obtaining the background absorbance. The Kubelka-Munk function $F(R_\infty)$ was calculated from the absorbance of the UV-vis spectra. The edge energy (E_g), or band gap, was determined by finding the intercept of the straight line for the low-energy rise of a plot of $[F(R_\infty)hv]^2$ versus hv, where hv is the incident photon energy. An example of this calculation can be found elsewhere.[30] For the *in situ* UV- vis

experiments, the supported 8%WO_x/SiO_2 catalyst was dehydrated at 500°C in 10% O_2/Ar before the temperature was lowered to 300°C under the flow of the same gas and the first spectrum was taken. The gas flow was then switched to Ar and then to 1% C_3=/He. The *in situ* UV-vis spectra were collected at 300, 350 and 400°C under flowing 1% C_3=/He. The catalyst was allowed to stabilize for 30 minutes at each reaction temperature before the spectrum was recorded. The flow rate of 30 mL/min is used for all gases in these *in situ* experiments.

2.3. *In situ* and *operando* Raman Spectroscopy

The Raman spectra of silica supported tungsten oxide catalysts were obtained with a Horiba-Jobin Ybon LabRam HR instrument equipped with three laser excitations (532, 442 and 325 nm) and a liquid N_2-cooled CCD detector (Horiba-Jobin Yvon CCD-3000V). The 442 nm laser was chosen since it minimized sample fluorescence. Spectral resolution was approximately 2 cm^{-1} and the wavenumber calibration was checked using the silica standard line at 520.7 cm^{-1}. The lasers were focused on the samples with a confocal microscope using a 50X objective (Olympus BX-30-LWD). Typically, the spectra were collected for 30 s/scan and 5 scans with a 200 μm hole. Approximately 5-25 mg of each catalyst in powder form was loaded into an environmental cell (Harrick, HVC-DR2) with a SiO_2 window and O-ring seals which was kept cool by flowing water. The *in situ* Raman spectra of the dehydrated catalysts were collected at room temperature after 500°C dehydration in 10% O_2/Ar for 30 minutes. A flow rate of 30 mL/min of 1% propylene/Ar (balance) was used for the *operando* Raman studies during propylene metathesis at 300°C. The gaseous effluent was simultaneously recorded with an online mass spectrometer (Varian, 1200L quadrupole).

2.4. *In situ/Operando* XAS (XANES/EXAFS) Spectroscopy

W L_1 -edge X-ray absorption spectroscopy (XAS) measurements were performed in transmission mode at the beamlines X19A and X18B at the National Synchrotron Light Source (NSLS) at the Brookhaven National Laboratory, using ionization chamber detectors for measuring incident and transmitted beam intensities. In addition, a third ionization chamber was used to detect the beam through a reference W foil for energy calibration and alignment purposes. A quartz capillary cell (I.D./O.D. = 0.8 / 1.0 mm) was used for *in situ* dehydrated measurements. Data processing and analysis were performed using Athena and Artemis software. The *in situ* XAS spectra of the dehydrated catalysts were collected at the reaction temperature of 300°C after 500°C dehydration in 20%O_2/He for 30 minutes. Reference compounds, $Ce_2(WO_4)_3$ (Strem, 99.9%), $H_3PW_{12}O_{40}$*nH_2O (Sigma Aldrich, 99.995%) and WO_3(Alfa Aesar, 99.8%) are diluted with Boron Nitride to have a metal loading of 2-5% and measured under ambient conditions. Only tungstophosphoric acid, $H_3PW_{12}O_{40}$*nH_2O (also diluted with Boron Nitride) was measured under both ambient and dehydrated conditions (150°C in 20% O_2/He for 30 minutes). This dehydration was performed to remove adsorbed moisture. For the *in situ* XAS experiments, after the aforementioned dehydration procedure, the catalysts were cooled down to 300°C in He. Then a flow of 1% $C_3^{=}$/He was introduced at the rate of 10 mL/min and the spectra were recorded as a function of time. The gaseous products were simultaneously analyzed online with a residual gas analyzer (RGA, Stanford Research System).

2.5. Temperature programmed surface reaction (TPSR) spectroscopy

The temperature programmed surface reaction experiments were performed using an Altamira Instruments (AMI-200) system. The outlet gases were connected to an online mass

spectrometer (Dymaxicon Dycor, (DME200MS) and a TCD detector for analysis. Typically, ~100-300mg of catalyst was loaded into the U-tube reactor. Blank tests with known concentrations of olefins were run for the mass spectrometer (MS) calibration before the experiments. The signals for the mass spectra were also normalized with catalyst weight for comparison. The following MS m/z values were used for detection of the reactants and products: propylene (m/z= 42), ethylene (m/z= 27), 2-butene (m/z=56), acetaldehyde (m/z=43), formaldehyde (m/z=30), carbon dioxide (m/z=44), acetone (m/z= 58), O_2 (m/z=32) and water (m/z=18). The MS cracking patterns were carefully determined with blank runs using the calibration gases and used to correct for the background MS signals. Cracking of propylene gives rise to m/z =43 and the propylene cracking contributions to CH_3CHO (m/z=43) were subtracted from the final MS signals. Cracking of 2- butene gives rise to m/z=27, 28, 30 and 41 values. Unless otherwise noted, the catalysts were dehydrated in 10% O_2/Ar at 500°C (30 mL/min) for 30 minutes and cooled in flowing Ar (30 mL/min) to the reaction temperature. The desired reactant amount is achieved by diluting the 5% C_3=/Ar with additional Ar.

2.6. Steady-State Reaction Studies

The catalytic activity measurements were performed in a fixed-bed catalytic reactor under differential conditions (propylene conversion <15%). A separate molecular sieve moisture trap was installed in the inlet propylene gas line to purify the reactants. Both inlet and outlet gas lines were heated using external electric heaters to ~200°C to prevent condensation of the reactants and products. The catalysts were pretreated in 10% O_2/Ar at 500°C for 30 minutes before cooling down in Ar to 300°C. Then a gas mixture of 1% C_3H_6/Ar was introduced at the rate of ~100mL/min. The products were analyzed using an online gas chromatograph (Agilent

GC 6890) equipped with flame ionization (Agilent Serial #: USC250823H) and thermal conductivity (Restek Product #: PC3533) detectors. Conversion was normalized with propylene flow rate and catalyst weight to obtain the propylene metathesis reactivity (mmol/g/hr). The reactivity is computed from

$$\text{reactivity}\left(\frac{\text{mmol}}{\text{g}*\text{hr}}\right)=\frac{\text{Conversion}*\text{Concentraion}*\text{Flowrate}\left(\frac{\text{mL}}{\text{min}}\right)*\left(60\frac{\text{min}}{\text{hr}}\right)*\left(\frac{1}{1000}\frac{\text{L}}{\text{mL}}\right)}{\left(22.4\frac{\text{L}}{\text{mol}}\right)*\text{LoadingWeight(g)}} \quad (1)$$

The conversion of propylene is computed from the change of its GC area with and without the catalyst at each reaction condition. Selectivity of a product (S_i) is obtained from dividing its GC area (x_i) from the total area of all products, X (excluding the reactant propylene), which can mathematically be expressed as

$$S_i=\frac{x_i}{X}\times 100 \quad (2)$$

3. Results

3.1. *In situ* UV-vis Spectroscopy

The *in situ* UV-vis Eg values of the dehydrated supported WO_x/SiO_2 catalysts along with those of references are shown in Figure 1. The reference Eg values for tungsten oxide isolated and oligomeric structures are taken from reference 20. Distortion of isolated WO_4 sites has a modest effect and decreases the Eg value from 4.6 to 4.2 eV. Below 8% WO_x/SiO_2, the Eg values for the dehydrated catalysts are ~4.2-4.3 eV indicating the presence of isolated WO_x sites on the silica support. Above 6% WO_x/SiO_2, the Eg value monotonically decreases from ~4.2 to 3.4 eV with increasing tungsten oxide loading. The decreasing Eg values reflect the presence of

larger WO_x domains and are related to the presence of crystalline WO_3 nanoparticles (NPs) in these catalysts, which will be shown below with the corresponding Raman spectroscopy.

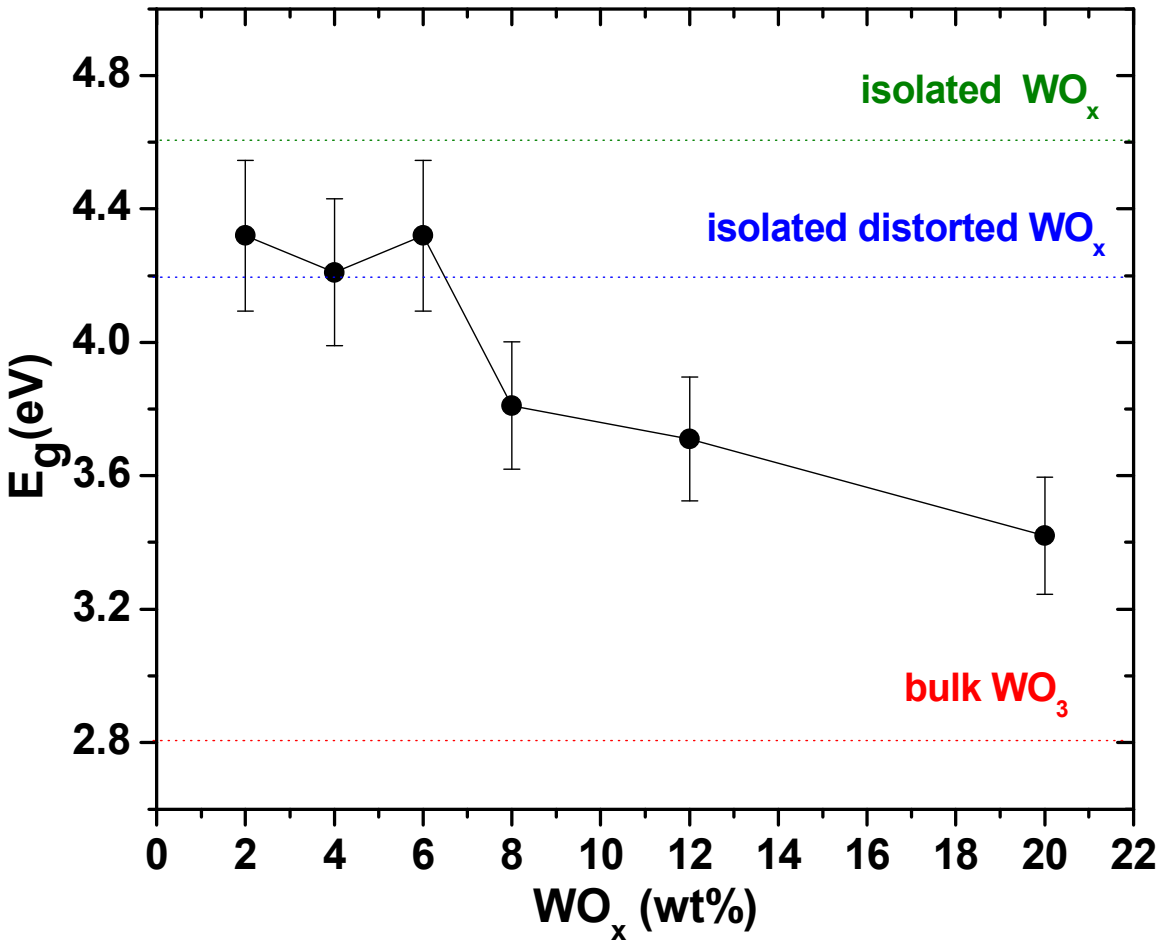

Figure 1. *In situ* UV-vis Eg values for the dehydrated supported WO_x/SiO_2 catalysts as a function of surface tungsten oxide coverage with those of reference compounds.

The *in situ* UV-vis spectra during the propylene metathesis reaction are presented in Figure 2a. The curves in flowing O_2/Ar and Ar are identical and only the latter is evident in Figure 2a since the Ar curve overlaps the O_2/Ar curve. The difference spectra in Figure 2b were

obtained by subtracting the fully oxidized spectrum from the spectra during reaction. Introducing Ar after the O_2/Ar pretreatment does not form UV-vis d-d bands of reduced WO_x in the 300-800 nm region indicating that the WO_x sites on SiO_2 do not undergo detectable reduction in the inert environment. During propylene metathesis, the intensity of the W^{+6} LMCT band at ~260 nm decreases and weak d-d band(s) from reduced WO_x sites appear in the ~300-800 nm region. The UV-vis spectra of reduced WO_x compounds give rise to d-d transitions: W^{+5} in tris(pyrazolyl)borato-oxo-tungsten and $(Et_4N)[WO(S_2C_2Ph_2)_2]$ complexes exhibit bands at 470 and 720 nm [31,32] and W^{+4} in the WO_2 reference compound exhibits broad bands at 410 and 460 nm (see Figure 2b). The weak and broad UV-vis bands in the difference spectra during reaction suggest that some reduced surface W^{+5} and W^{+4} sites are present during propylene metathesis, but these weak and broad bands are not well-resolved to assign. The absence of strong UV-vis d-d bands for reduced surface WO_x sites probably reflects the oxidation of the reduced surface WO_x sites by the surface intermediates back to W^{+6} (see section below on catalyst activation). The presence of W^{+5} sites have been reported for olefin metathesis over supported WO_x/Al_2O_3 and WO_x/ZrO_2[33,34] catalysts with EPR spectroscopy. EPR spectroscopy, however, can't detect W^{+4} sites since they are not paramagnetic. These EPR measurements did not detect W^{+3}, which is paramagnetic, and reflect the absence of W^{+3} sites during olefin metathesis by supported WO_x catalysts.

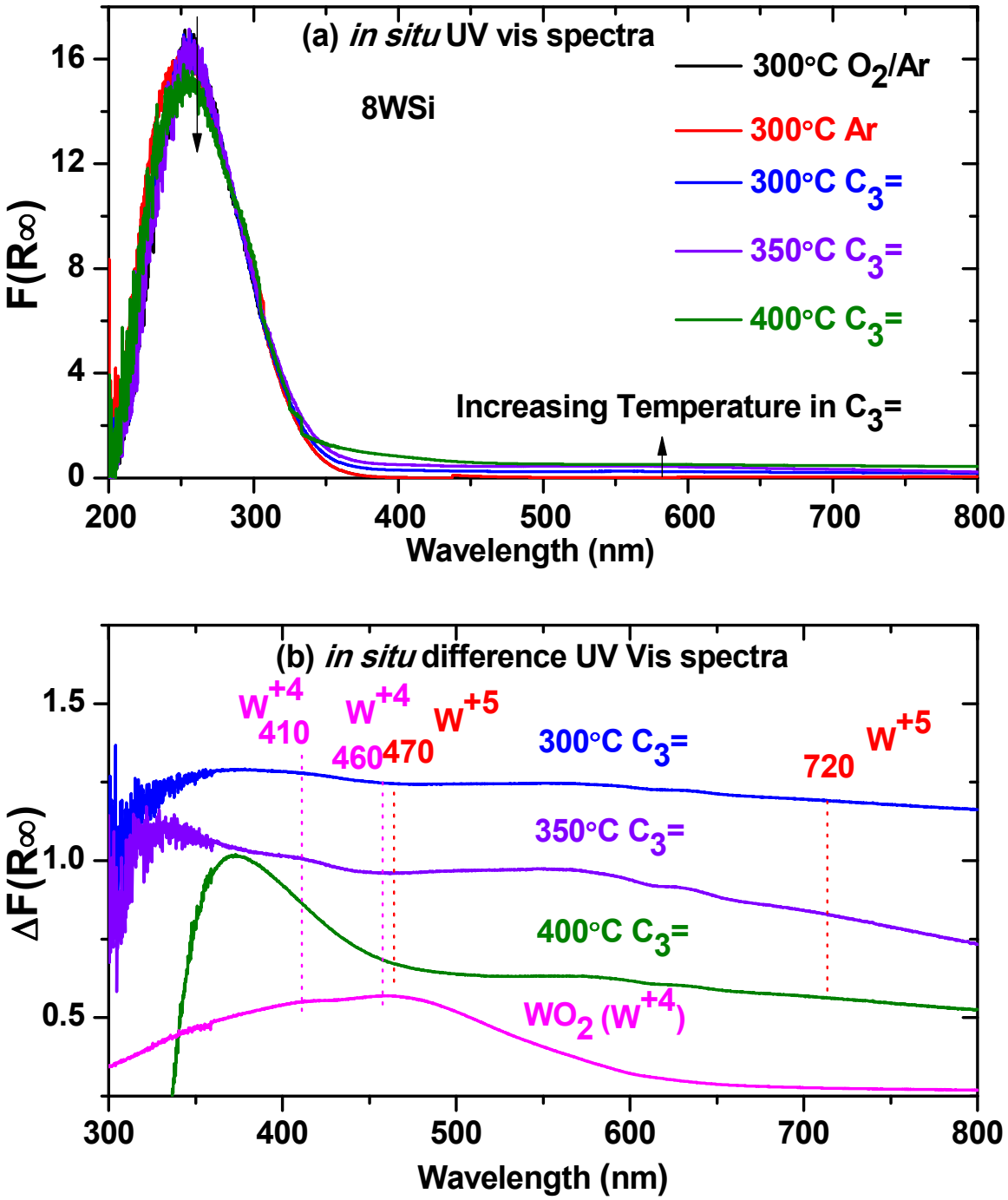

Figure 2. *In situ* UV-vis spectra of the supported 8%WO_x/SiO_2 catalyst (a) during propylene metathesis and (b) difference spectra along with that of the bulk WO_2 reference compound.

3.2. *In situ* W L_1-XANES and EXAFS Spectroscopy

The *in situ* W-L_1 XANES spectra of several reference materials with known structures and the dehydrated supported WO_x/SiO_2 catalysts are presented in Figure 3. The intensity of the XANES pre-edge peak increases when the absorbing atom (W) is displaced from the inversion symmetry center, resulting in a strong pre-edge feature for WO_4 coordinated structures and a weak pre-edge feature for WO_6 coordinated structures.[35,36] The bulk $Ce_2(WO_4)_3$ reference compound contains only isolated WO_4 sites[37] and, consequently, its XANES spectrum has a strong pre-edge feature. Bulk crystalline WO_3 is composed of WO_6-coordinated units with a more symmetric environment and, thus, its XANES pre-edge feature is quite small. Dehydrated crystalline $H_3PW_{12}O_{40}$ contains highly distorted mono-oxo WO_6 sites that deviate from the more symmetric environment of WO_3 giving rise to a weak XANES pre-edge peak. The dehydrated supported 4% WO_x/SiO_2 catalyst exhibits almost the same pre-edge intensity as bulk $Ce_2(WO_4)_3$. Comparison of the intensity of the XANES pre-edge peaks for the dehydrated supported 4% WO_x/SiO_2 catalyst and $Ce_2(WO_4)_3$ suggests that the catalyst contains ~92% WO_4-coordinated and ~8% WO_6-coordinated sites. The intensity of the XANES pre-edge for the supported 8% and 20% WO_x/SiO_2 catalysts decreases with tungsten oxide loading reflecting the additional presence of a WO_6-coordinated structure, which is crystalline WO_3 nanoparticles (NPs) (see Raman section below). Comparison of the XANES pre-edge intensity of the supported 8 and 20% WO_x/SiO_2 catalysts with that of the supported 4% WO_x/SiO_2 catalyst suggests that the catalysts with higher tungsten oxide loading contain ~25 and ~60% WO_3 NPs, respectively.

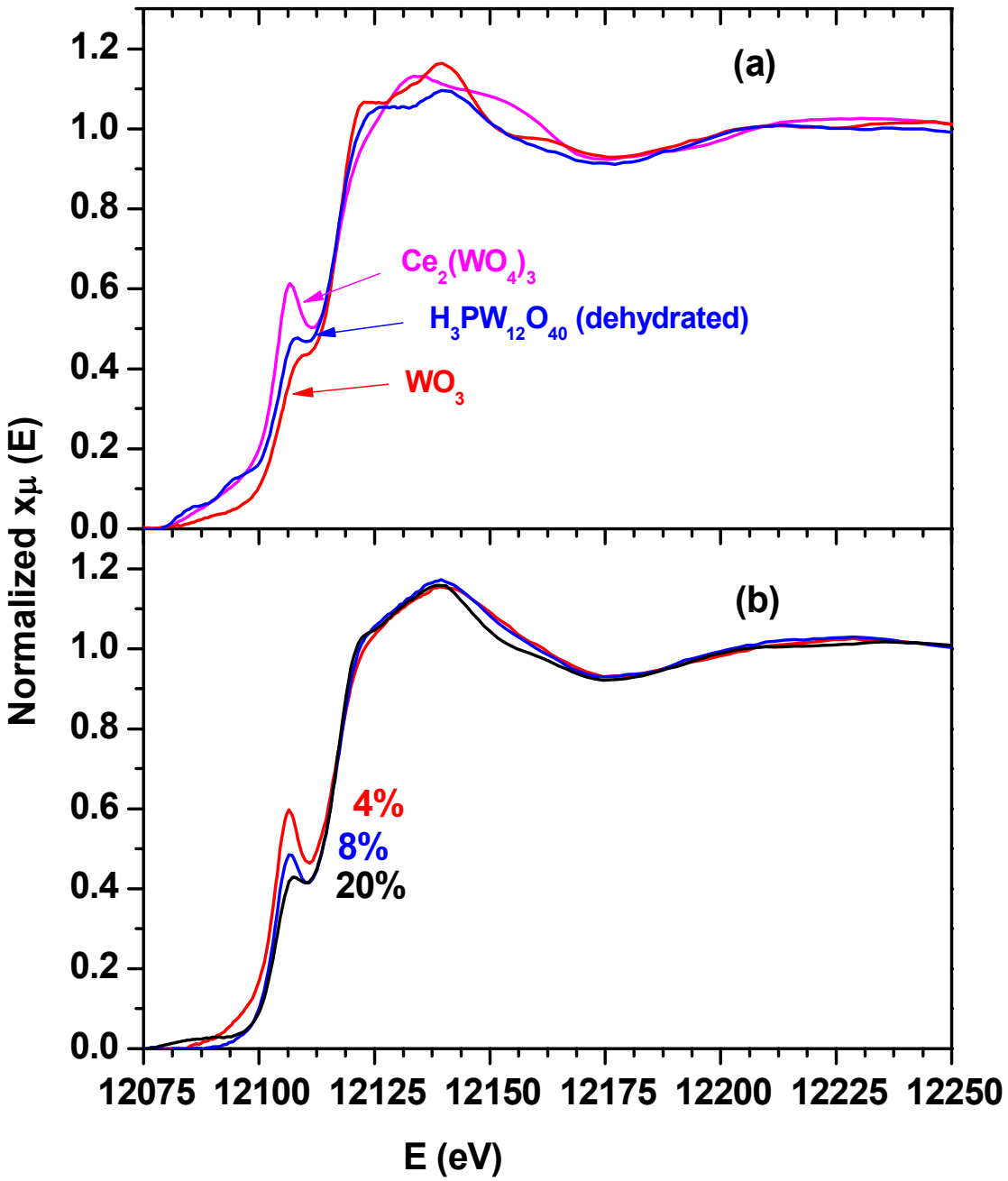

Figure 3. *In situ* W L_1 edge XANES spectra of (a) reference materials and (b) dehydrated supported WO_x/SiO_2 catalysts.

The corresponding *in situ* W L_1 EXAFS spectra provide information about the radial distribution of W-O bonds. The k^2 -weighted EXAFS spectra of the reference materials and dehydrated supported WO_x/SiO_2 catalysts are shown in Figure 4. All spectra exhibit distinct peaks assigned to W-O contribution in the range of 1-2 Å. As shown in Figure 4a, there are differences in W-O peak intensities and positions, reflecting the differences in W-O coordination environments between different reference compounds. The EXAFS spectra of the dehydrated supported WO_x/SiO_2 catalysts (Figure 4b) exhibit similar spectral features. The intensity of W-O peak (at ~ 1.2 Å) is dependent on WO_x loading, suggesting the coordination number or/and distribution of W-O bond changes as a function of WO_x loading. To obtain quantitative information on W-O bonding environment, EXAFS analysis of the reference $Ce_2(WO_4)_3$ and the dehydrated supported WO_x/SiO_2 catalysts were performed. First, we analyzed the $Ce_2(WO_4)_3$ compound in order to obtain the amplitude factor (found to be 0.64±0.09), assuming the tetrahedral coordination of W by O atoms. Then, the amplitude factor was fixed to 0.64 and applied to all data sets of catalysts. We performed fitting of all catalysts simultaneously and examined two models: 1) varying the coordination number (N) of W-O bonds while requiring that the disorder factor (σ^2) of W-O bond is the same for all the data sets, and 2) varying both N and σ^2 for all the data. The fitting quality using the two models is comparable, and they have similar reduced Chi-squared and R-factors. Due to the strong N - σ^2 correlation, the W-O coordination number could not be obtained reliably from EXAFS analysis, but the best fit values of the W-O bond distances provided important insights. In the both analysis models, the average W-O bond distances are found similar for all WO_x/SiO_2 catalysts (1.83±0.02 Å for 4%, 1.87±0.03 Å for 8% and 1.82±0.02 Å for 20% WO_x/SiO_2) suggesting that all the catalysts are dominated by a W-O short bond that is known to be present for surface WO_x sites on SiO_2.[22]

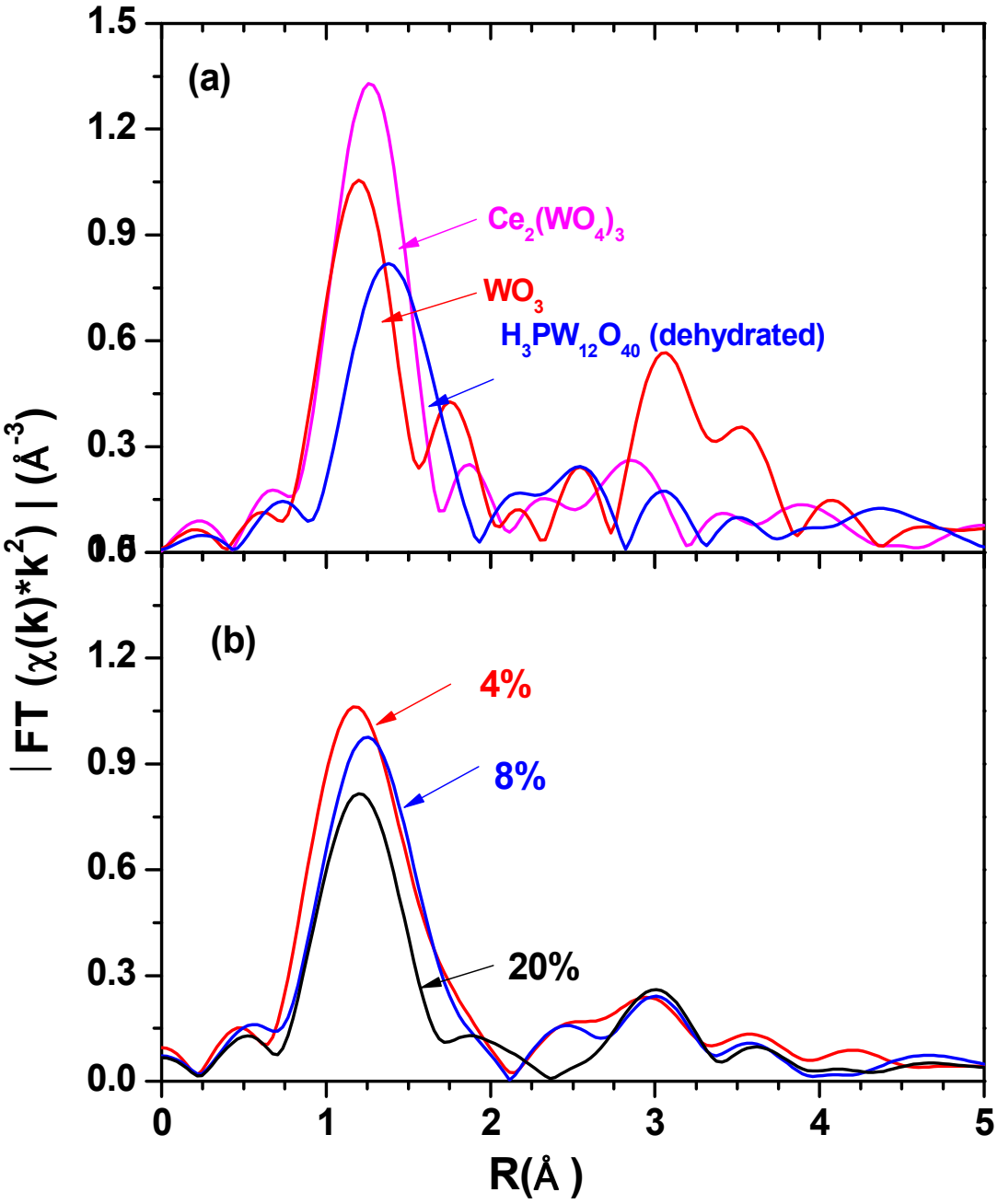

Figure 4. Magnitudes of Fourier-transformed, not-phase-corrected, k^2-weighted W L_1-edge EXAFS spectra in the *R* space for the (a) reference materials and (b) dehydrated supported WO_x/SiO_2 catalysts. For all the data, the *k* range for Fourier transformation is 2-9 $Å^{-1}$.

The *in situ* XANES spectra of the supported 4% and 20% WO_x/SiO_2 catalysts during propylene metathesis at 300°C are shown in Figure S1. The supported 4%WO_x/SiO_2 catalyst is free of WO_3 NPs (see UV-vis section above and Raman section below) and exhibits almost no decrease in the intensity of the XANES pre-edge peak during propylene metathesis. The supported 20% WO_x/SiO_2 catalyst that contains a significant amount of crystalline WO_3 NPs (UV-vis section above and Raman section below), however, it also does not exhibit an apparent decrease in the intensity of the XANES pre-edge peak during propylene metathesis. The k^2 weighted W L_1-edge EXAFS data of the supported WO_x/SiO_2 catalysts are presented in Figure S2 and do not undergo any significant changes. The corresponding *operando* MS spectra for both catalysts are shown in Figure S3.

3.3. *In situ/Operando* Raman Spectroscopy

The *in situ* Raman spectra of the dehydrated supported WO_x/SiO_2 catalysts before olefin metathesis are presented in Figure 5. The Raman spectra are normalized with respect to the 495 cm^{-1} band of the SiO_2 support. The silica support gives rise to Raman bands at 410-415, 487, 605, 810 and 970 cm^{-1} that have been assigned to network bending modes, D1 and D2 defect modes related to tri- and tetra-cycloxiloxane rings, Si-O-Si symmetrical stretching and Si-OH stretching mode of the surface hydroxyls, respectively.[22] The supported 4% and 6% WO_x/SiO_2 catalysts exhibit additional Raman bands at 1016, 985 and 350 cm^{-1} from dioxo v_s $[(O=)_2WO_2]$ stretch, mono-oxo v_s $[O=WO_4]$ stretch and their associated bending modes at ~350 cm^{-1}, respectively.[22] The small shoulder at ~968 cm^{-1} is the v_{as} $[(O=)_2WO_2]$ vibrational stretch of the surface dioxo site. The ratio of the raw Raman bands for the dioxo/mono-oxo surface WO_x sites is ~1.5 and ~2.5 for the supported 2 and 4% WO_x/SiO_2 catalysts, respectively, and decreases to

~0.7 for supported 8 and 20% WO_x/SiO_2 catalysts (see Figures S4a and S4b in SI). Switching the gaseous environment from He to O_2/He has a minimal effect on the dioxo/mono-oxo ratio (see Figure S5). The absence of Raman bands from bending W-O-W vibrations in the ~200-300 cm^{-1} region demonstrates that the surface WO_x sites are isolated, which is in agreement with the UV-vis findings above. Crystalline WO_3 NPs (Raman bands at ~265, ~325, ~715 and ~806 cm^{-1}) have a Raman cross-section that is significantly stronger than the surface WO_x sites,[38] and are not present for the supported 4% and 6% WO_x/SiO_2 catalysts, but are clearly present for supported 8% WO_x/SiO_2 and higher tungsten oxide loadings. The Raman bands of the symmetric stretches of the surface dioxo WO_4 and mono-oxo WO_5 sites slightly blue shift in the presence of the crystalline WO_3 NPs. The Raman spectra reveal that tungsten oxide is 100% dispersed on SiO_2 below 8% WO_3/SiO_2 for the current set of synthesized catalysts, which is in agreement with the above UV-vis findings.

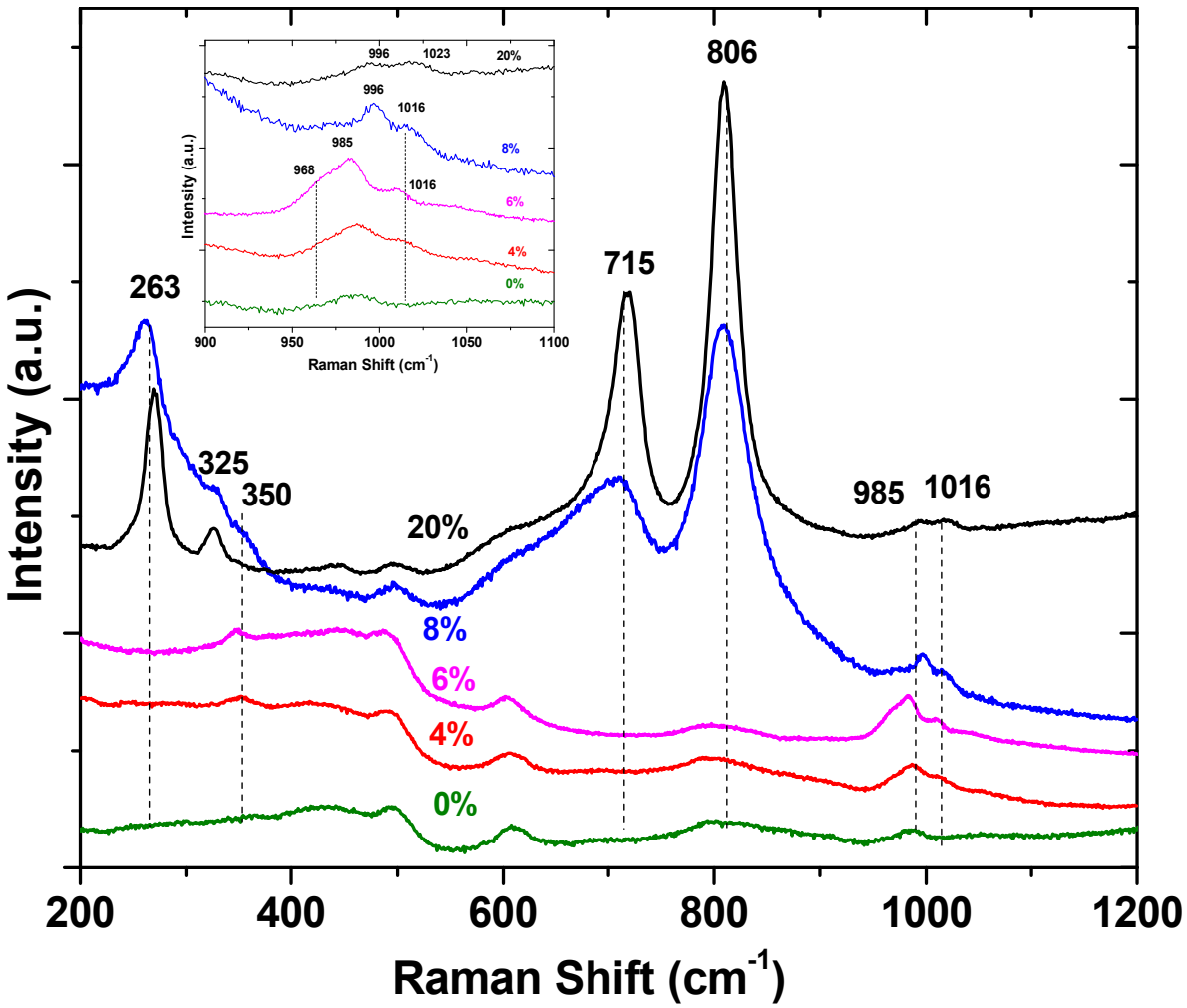

Figure 5. *In situ* Raman spectra (442 nm) of the supported WO_x/SiO_2 catalysts under dehydrated conditions (flowing O_2/Ar at 300°C). Inset shows the 900-1100 cm^{-1} region.

The *operando* Raman spectra of the supported 4% and 8% WO_x/SiO_2 catalysts during propylene metathesis are presented in Figures 6 and 7 with the bands normalized by employing the SiO_2 vibrations at 815 cm^{-1} for the 4% catalyst and 495 cm^{-1} for the 8% catalyst as internal standards. The strong 805 cm^{-1} band for WO_3 crystals prevents monitoring of the SiO_2 815 cm^{-1} band as an internal standard for the 8%WO_x/SiO_2 catalyst. Therefore, the silica Raman band at

495 cm^{-1} band was used as an internal standard for 8%WO_x/SiO_2 catalyst. Prior to propylene metathesis, the catalyst were always flushed with flowing Ar to remove gas phase molecular O_2 before beginning the flow of $C_3^=$/Ar. The Raman spectra in flowing 10% O_2/Ar and Ar were the same in both environments. The *in situ* Raman spectra of the supported 4% WO_x/SiO_2 catalyst (Figure 6a) indicate that the intensity of the Raman bands of both surface dioxo $(O=)_2WO_2$ and mono-oxo $O=WO_4$ sites decrease during propylene metathesis and both bands are present for at least ~100 minutes of reaction. The intensity of the Raman bands from both surface WO_x sites selectively decrease with reaction time relative to the irreducible SiO_2 support. This indicates that both surface WO_x sites have been activated by loss of W=O oxo bonds formation of surface $W=CH_2/W=CHCH_3$ intermediates and that the intensity decrease is not related to deposition of carbonaceous deposits. The decrease in W=O vibrations is due to removal of oxygen and coordination of olefins and their reaction intermediates to the surface WO_x sites. Within experimental error, it is difficult to determine if one of the surface WO_x sites reduces faster than the other. The corresponding simultaneous MS signals confirm that the propylene metathesis reaction is taking place and that the MS ratio of $C_2^=/C_4^=$~1. Both surface WO_x sites remain dispersed on the silica support during propylene metathesis since reoxidation does not reveal crystalline WO_3 NPs and the relative ratio of the surface dioxo/mono-oxo is the same at the beginning of the reaction and after reaction, The behavior of crystalline WO_3 NPs during propylene metathesis is presented in Figure 7 for the supported 8% WO_x/SiO_2 catalyst. The intensity of the Raman bands for the crystalline WO_3 NPs monotonically decreases with propylene metathesis reaction time indicating reduction of these sites. Complete recovery of the intensity of the Raman bands from the crystalline WO_3 NPs is obtained upon reoxidation indicating that the loss in intensity is related to reduction of the crystalline WO_3 NPs during

metathesis. The corresponding simultaneous MS signals show that propylene metathesis is taking place with a ratio of only $C_2^=/C_4^=$~0.1. The almost order of magnitude decrease in formation of ethylene must be related to the significant amount of crystalline WO_3 NPs in the support 8% WO_x/SiO_2 catalyst (~25%) since it is the only difference between the type of tungsten oxide sites in the supported 8% and 4% WO_x/SiO_2 catalysts. The formation of some polyaromatic coke on both catalysts is reflected by Raman bands at 1350 cm^{-1} and 1600 cm^{-1}(SI Figure S6).

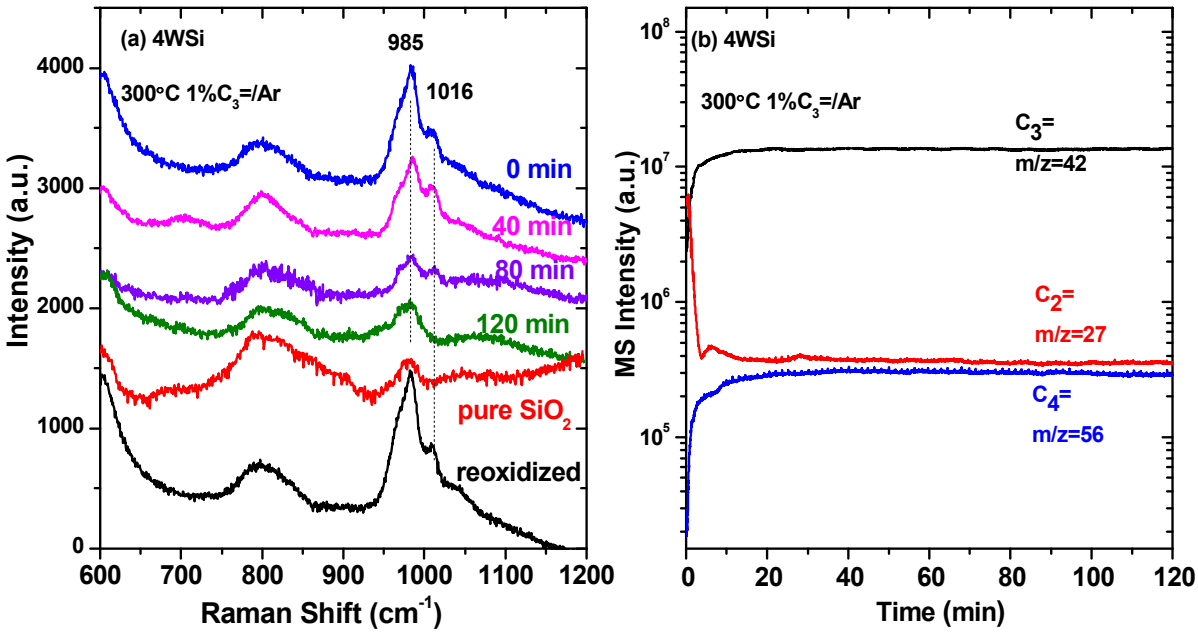

Figure 6. (a) *Operando* Raman spectra (442 nm) of the supported 4%WO_x/SiO_2 catalyst (Raman spectrum of pure SiO_2 is shown for comparison) at 300°C, and (b) its simultaneous MS spectra for main products. The catalyst was reoxidized in 10% O_2/Ar at 500°C for 30 minutes after the reaction (Raman spectra normalized against SiO_2 band at 815 cm^{-1}). Propylene conversion was ~4%.

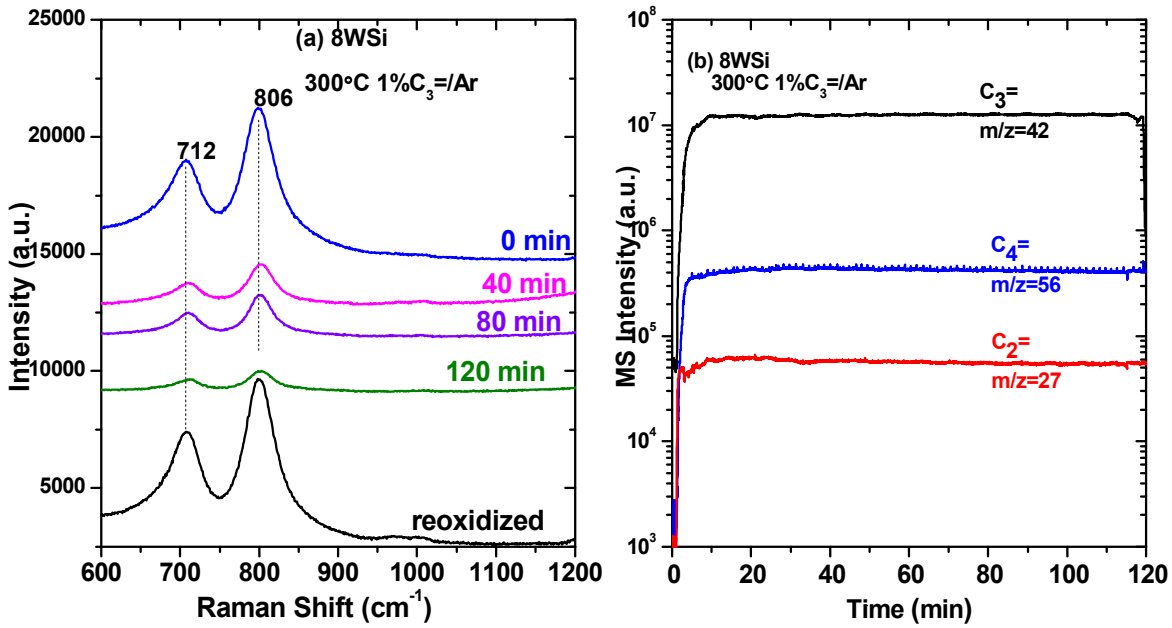

Figure 7. (a) *Operando* Raman spectra (442 nm) of the supported 8%WO_x/SiO_2 catalyst at 300°C, and (b) simultaneous MS spectra for the main products. The catalyst was reoxidized in 10% O_2/Ar at 500°C for 30 minutes after the reaction (Raman spectra normalized against SiO_2 band at 495 cm^{-1} because of strong WO_3 band at 806 cm^{-1}). Propylene conversion was ~9%.

3.4. Activation of Supported WO_x/SiO_2 Catalysts at Constant Temperature (500°C)

The supported 8% WO_x/SiO_2 catalyst was activated by exposure to flowing $C_3^=$/Ar at 500°C and the results for the first 60 minutes are presented in Figure 8. The initial product is a spike of O_2 most probably from displacement of a small amount of residual oxygen from the reactor by the flowing $C_3^=$/Ar. Immediately afterwards, the metathesis of propylene to ethylene and butene reaction began and oxygenated products (CH_3CHO, HCHO, H_2O and CO_2) also appear. Note that the oxygenated product acetone, CH_3COCH_3, was not detected.

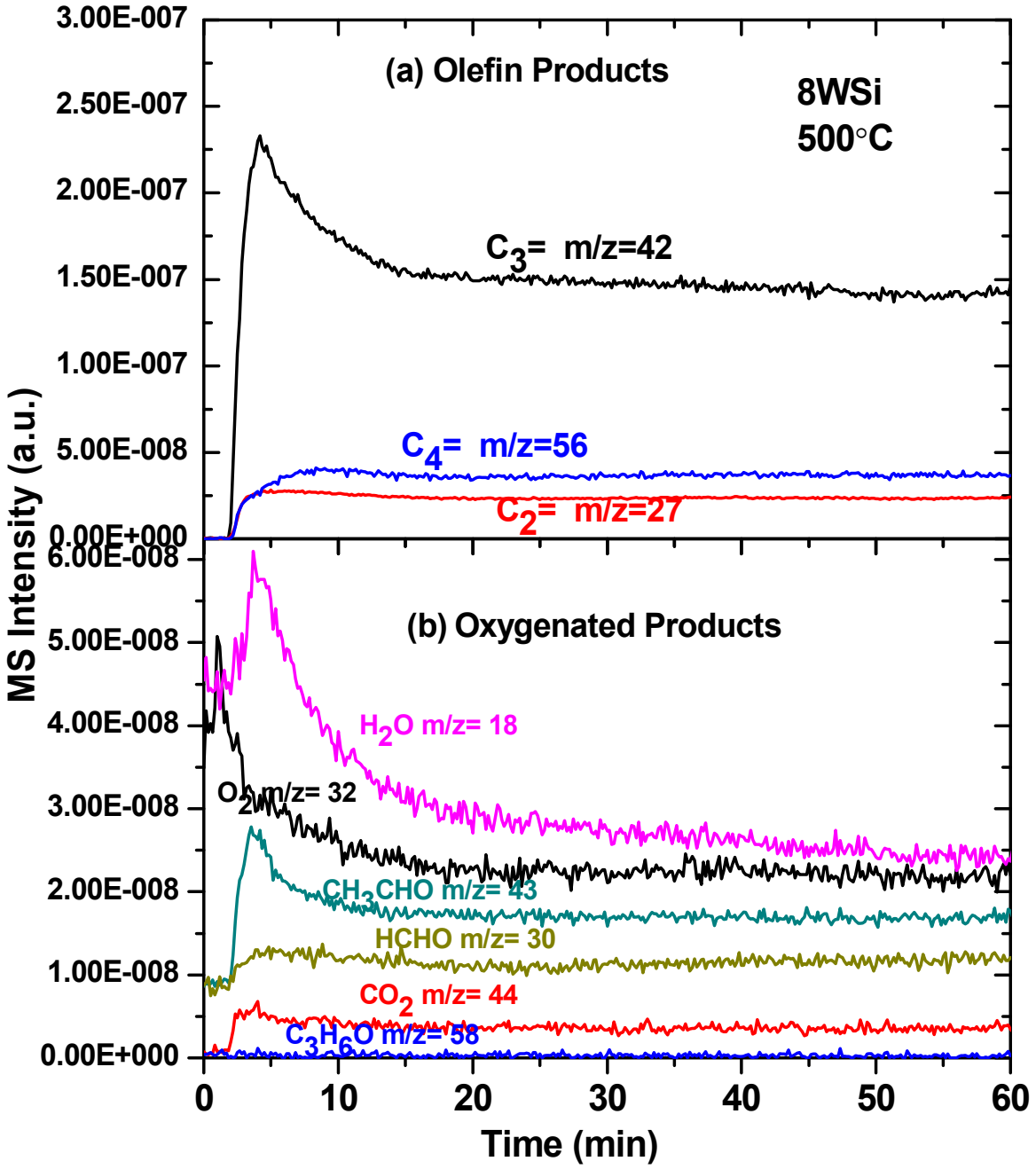

Figure 8. Activation of supported 8% WO_x/SiO_2 catalyst by flowing 1% C_3=/Ar at 500°C: (a) olefin products and (b) oxygenated products. Propylene conversion was ~18%.

3.5. Activation of Supported WO_x/SiO_2 Catalysts during TPSR spectroscopy

The production of $C_4^=$ during activation of supported WO_x/SiO_2 in flowing $C_3^=$ in the temperature programmed mode is presented in Figure 9 as a function of WO_x loadings. The $C_4^=$-TPSR spectra for the supported 4% and 8% WO_x/SiO_2 catalysts are very similar (same Tp value), with the 4% WO_x/SiO_2 catalyst being slightly more active at the lower temperatures. The lack of increased production of $C_4^=$ in going from the 4% WO_x/SiO_2 to the 8% WO_x/SiO_2 catalyst reveals that the crystalline WO_3 NPs in the latter don't play a significant role in olefin metathesis and may actually diminish $C_4^=$ formation. This is further confirmed for the production of $C_4^=$ during TPSR with the 20% WO_x/SiO_2 catalyst, which consists of ~65% WO_3 NPs, that yields even less formation of $C_4^=$. The leading edges for $C_4^=$ formation are almost the same for the 8% and 20% WO_x/SiO_2 catalysts.

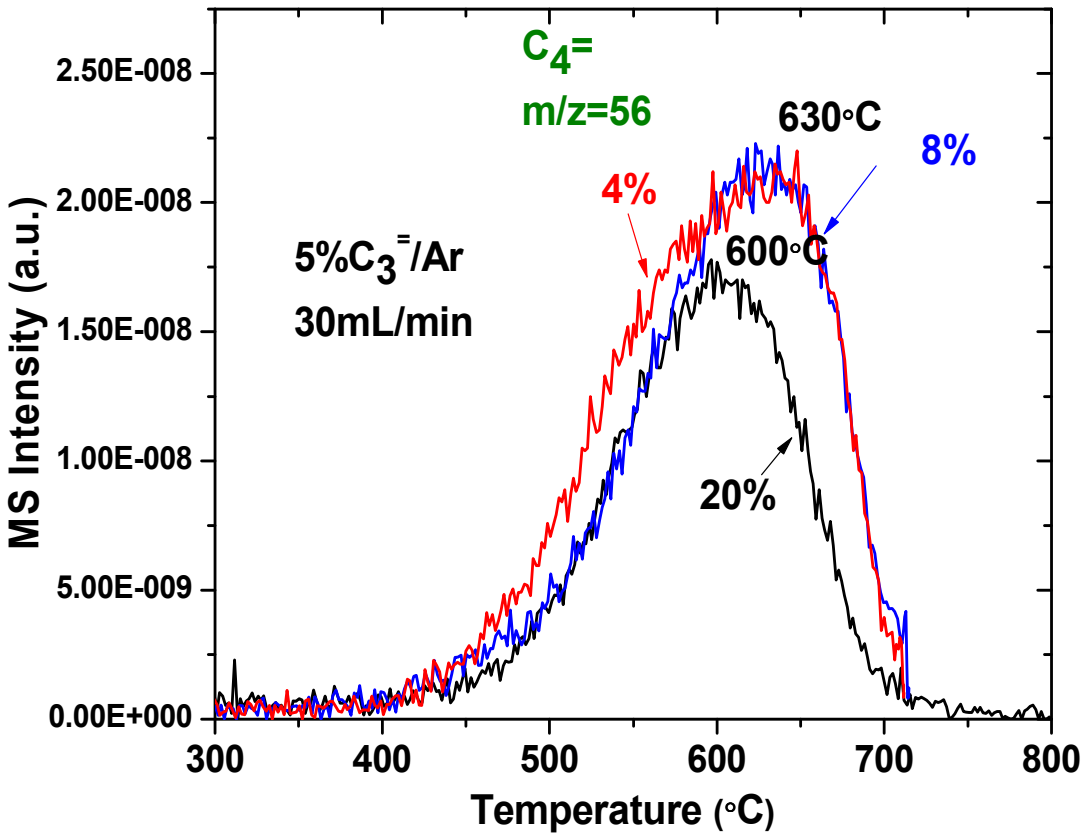

Figure 9. Production of $C_4^=$ during TPSR in flowing 5% $C_3^=$/Ar as a function of WO_x loadings. Other reaction products are shown in Figure S7.

The simultaneous evolution of H_2O and CO_2 during $C_3^=$ activation in the TPSR mode is presented in Figure 10. Formation of these oxidation products confirms the removal of oxygen atoms from the supported tungsten oxide phases on silica. The characteristics of H_2O evolution is dependent on the tungsten oxide loading. The supported 4% WO_x/SiO_2 catalyst, only containing the isolated surface WO_x sites, evolves H_2O in one major peak with Tp=630°C. The higher loading catalysts, containing both isolated WO_x sites and WO_3 NPs, exhibit two H_2O peaks at ~485 and ~630°C. The production of H_2O at ~630°C is related to isolated surface WO_x sites on silica since this peak is observed for the 4% WO_x/SiO_2 catalyst that only contains isolated sites. The second H_2O peak at ~485°C, however, is associated with the WO_3 NPs and the intensity of this peak tracks their concentration in the catalysts. Integration of the H_2O-TPSR peaks indicates that the ~485°C peak accounts for ~40% and ~60% of the total H_2O produced for the 8% and 20% WO_x/SiO_2 catalysts. These values reasonably track the amounts of crystalline WO_3 in these catalysts estimated above from XANES analysis. The evolution of CO_2 initiates at ~600°C and peaks at ~680°C. The formation of H_2O below 600°C and formation of CO_2 above 600°C suggests that some carbonaceous deposits are present on the catalyst during activation of the supported WO_x/SiO_2 catalysts by propylene below 600°C

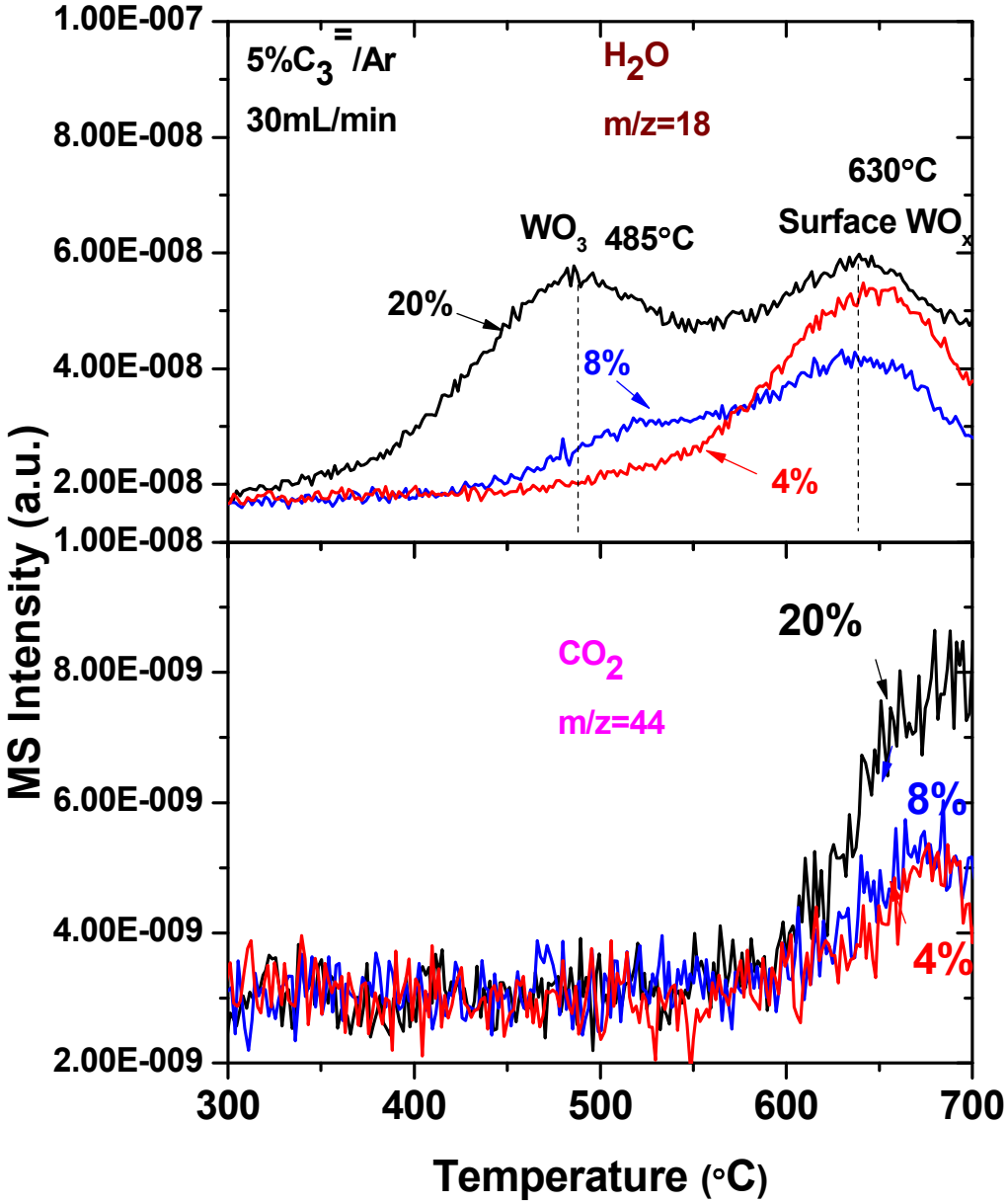

Figure 10. Production of H_2O and CO_2 in flowing 5% $C_3^{=}$/Ar as a function of WO_x loadings. The simultaneous conversion of $C_3^{=}$ and formation of $C_2^{=}$ are shown in Figure S7.

The influence of propylene in the gas phase on the supported 8% WO_x/SiO_2 catalyst pre-activated with propylene at 500°C for 45 minutes followed by additional exposure to propylene at 100°C for 45 minutes is presented in Figure 11. When the TPSR is performed in flowing $C_3^{=}$-

free Ar, no butene is formed. Performing TPSR in flowing $C_3^=$/Ar after the catalyst activation treatment produces butene at both ~220 and ~600°C. The $C_4^=$ peak at ~600°C is also observed during TPSR with an unactivated catalyst (see Figure 9), which suggests that the new low temperature $C_4^=$ peak is related to a new activated surface WO_x site. The $C_3^=$-TPSR findings also suggest that surface reaction intermediates are not stabilized on activated WO_x/SiO_2 catalysts and the metathesis reaction requires the presence of propylene in the gas phase in order to proceed.

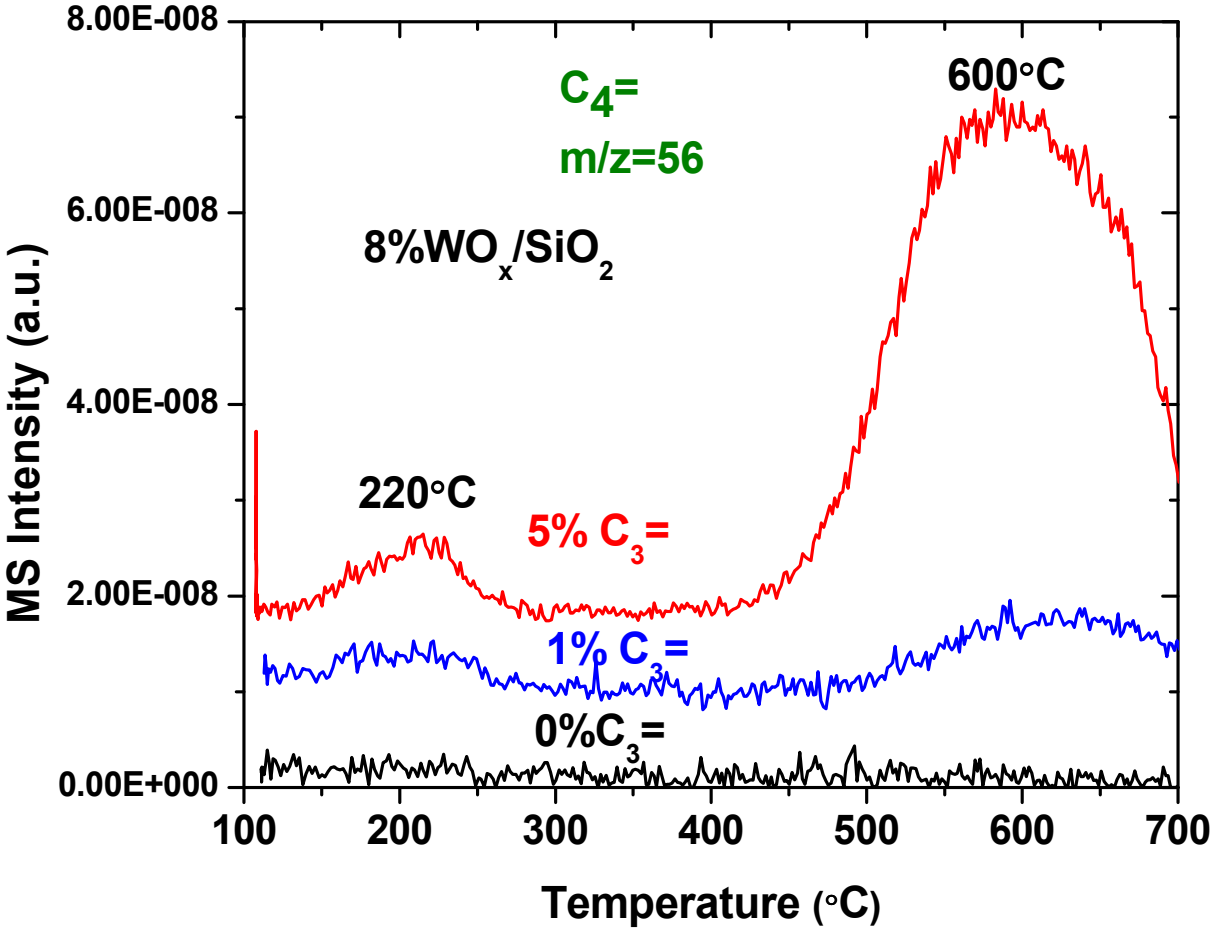

Figure 11. Production of $C_4^=$ during $C_3^=$-TPSR with 8% WO_x/SiO_2 catalyst in flowing $C_3^=$/Ar as a function of propylene concentration after a 500°C $C_3^=$/Ar treatment for 45 minutes and $C_3^=$.

adsorption at 100°C before starting the $C_3^=$-TPSR. Other reaction products are shown in Figure S8.

3.6. Steady-State Olefin Metathesis Reaction Studies

The reaction rates (propylene molecules converted per g-cat per hour) and selectivity for propylene metathesis by the supported WO_x/SiO_2 catalysts as a function of tungsten oxide loading are presented in Figures 12 and 13, respectively. The propylene metathesis reaction rate increases with tungsten oxide loading up to 8% WO_3/SiO_2 and then levels off for higher tungsten oxide loadings. Below 8% WO_3/SiO_2, only surface WO_x sites are present on the silica support and demonstrate that the reaction rate is proportional to the surface WO_x sites concentration (the catalytic active sites). Above 8% WO_3/SiO_2, the propylene metathesis reaction rate is relatively constant reflecting the lack of influence of the WO_3 NPs upon reaction rate (not the catalytic active sites). The propylene metathesis $C_2^=/C_4^=$ selectivity is sensitive to the nature of the tungsten oxide sites present in the catalyst. Below 8% WO_x/SiO_2, where only surface WO_x sites are present, the ratio of $C_2^=/C_4^=$ ~1 and ~20% C_4-C_6 alkane byproducts are also formed from the weak Lewis acidy associated with the surface WO_x sites on SiO_2.[39] The selectivity to C_4 and C_5 is relatively constant and the selectivity to C_6 increases with tungsten oxide loading from 2-6% WO_x/SiO_2. For 8% WO_x/SiO_2 and higher loadings, where crystalline WO_3 NPs are present in addition to the surface WO_x sites, the selectivity to $C_2^=$ dramatically decreases while the selectivity of $C_4^=$ modestly increases with tungsten oxide loading. The selectivity towards alkanes also further increases ($C_6 > C_5 > C_4$) with tungsten oxide loading with increasing amount of crystalline WO_3 NPs. These selectivity changes are thought to arise from the surface Brønsted acid sites associated with the crystalline WO_3 NPs.[40,41]

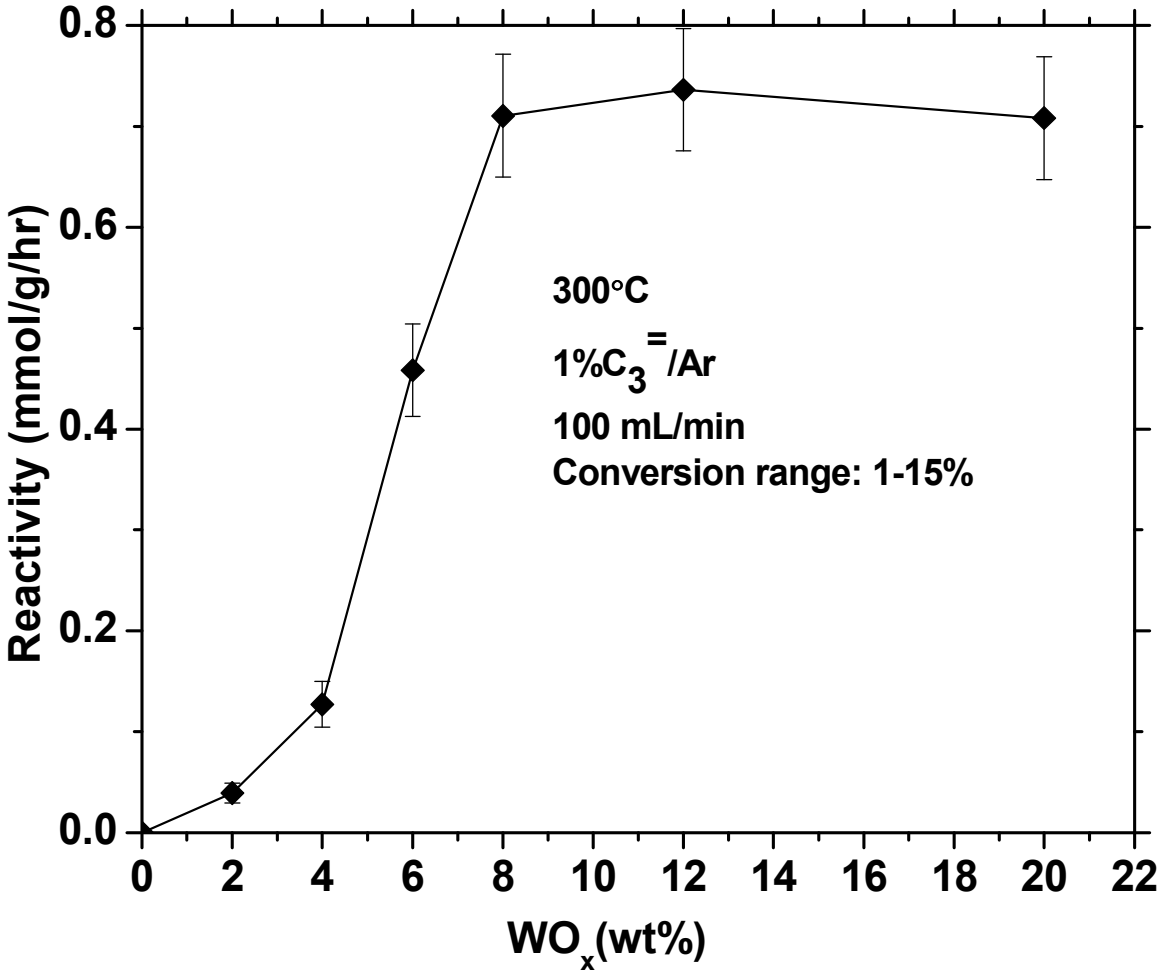

Figure 12. Propylene metathesis activity as a function of WO_x loadings for the supported WO_x/SiO_2 catalysts.

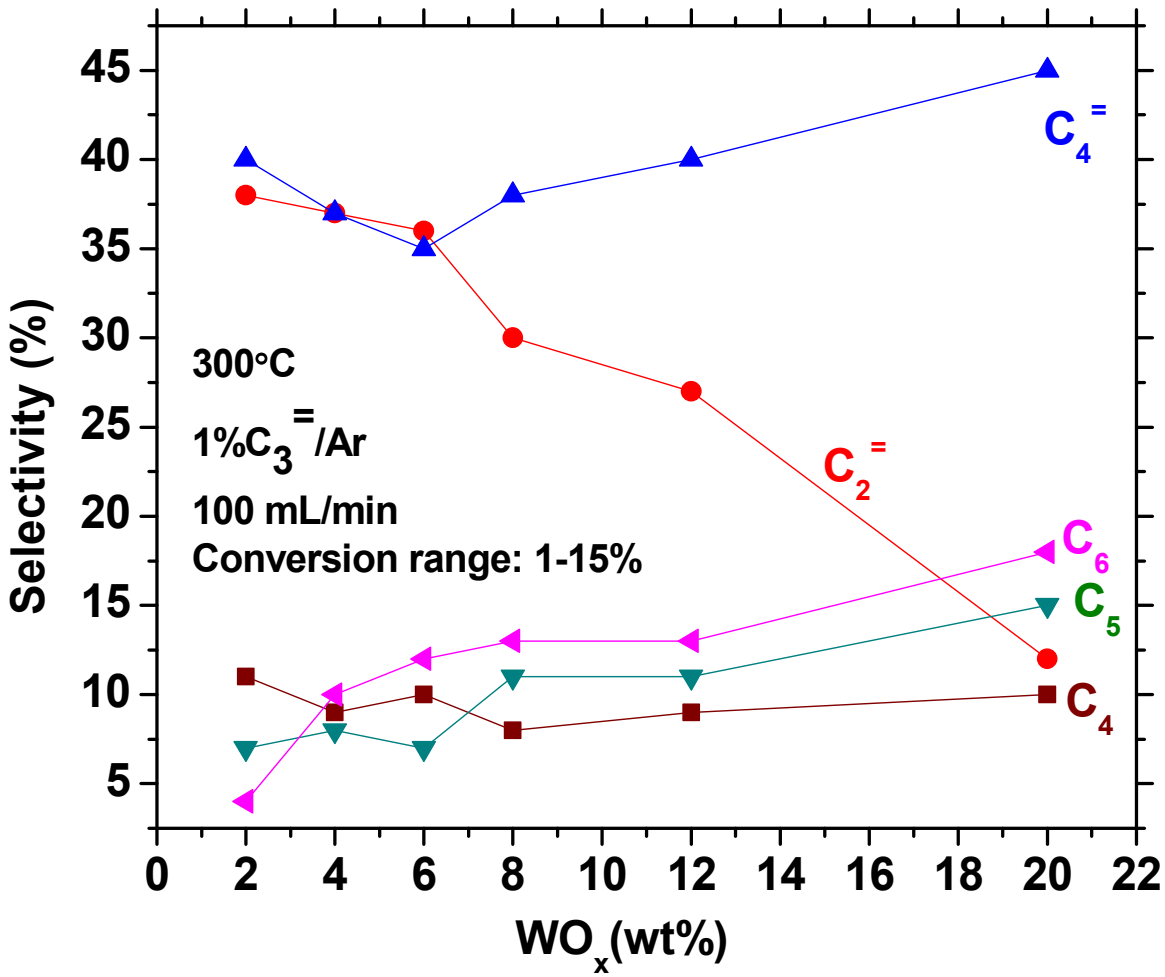

Figure 13. Propylene metathesis selectivity as a function of WO_x loadings for the supported WO_x/SiO_2 catalysts.

4. Discussion

4.1. Molecular structures of the dehydrated supported WO_x sites on SiO_2

Under dehydrated conditions**,** isolated surface WO_x sites and crystalline WO_3 NPs are present on the SiO_2 support with their relative concentrations varying with tungsten oxide loading. At the lower loadings (<8% WO_3/SiO_2), the isolated nature of the surface WO_x sites on silica is reflected by the high UV-vis Eg value (~4.2-4.3 eV), lack of detectable bridging W-O-W

Raman bending modes (~200-300 cm^{-1}) and absence of W in the EXAFS second coordination sphere (~3 Å). The surface WO_x sites are present as dioxo $(O=)_2W(-O)_2$ and mono-oxo $O=W(-O)_4$ with the concentration of the former much higher at lower tungsten oxide loadings (determined from the intensity of its *in situ* XANES pre-edge peak by comparison with reference compounds). For 8% WO_x/SiO_2 and higher tungsten oxide loadings, crystalline WO_3 NPs are also present in addition to the surface WO_x sites and their content increases with tungsten oxide loading (~25% for 8% WO_x/SiO_2 and ~60% for 20% WO_3/SiO_2). The appearance of WO_3 NPs coincides with the blue shift vibration for the surface WO_x sites, which may be related to their anchoring at more strained silica hydroxyl sites,[42] and a decrease in the dioxo/mono-oxo ratio. The ratio of dioxo/mon-oxo appears to be comparable in flowing O_2/He and He. In summary, two distinct surface WO_x sites are present on SiO_2 below 8% WO_x/SiO_2 and are accompanied with crystalline WO_3 NPs for 8% WO_x/SiO_2 and higher tungsten oxide loadings.

The literature for olefin metathesis by supported WO_x/SiO_2 catalysts seems to be confused about the molecular structures of the surface WO_x sites.[14-19] These publications assign the structure of the dehydrated surface WO_x sites on silica as being dioxo $(O=)_2W(-O)_2$, but their characterization measurements were performed under ambient conditions where the catalysts are wet and the sites are actually present as hydrated $W_{6-12}O_x$ clusters.[20,21] The current study, as well as our earlier publications,[20-23] reveal that two distinct isolated surface WO_x sites are present on SiO_2 at elevated temperatures where olefin metathesis is typically conducted with supported WO_x/SiO_2 catalysts.

4.2 Activation of surface WO_x sites and WO_3 NPs during metathesis

At lower tungsten oxide loadings, the surface WO_x sites are activated during propylene metathesis by loss of oxygen as shown by the (*i*) selective decrease in the intensity of the Raman bands for the supported WO_x sites (see Figure 6), (*ii*) appearance of UV-vis d-d bands (see Figure 2) and (*iii*) formation of oxygenated reaction products (see Figure 8). The decrease in the intensity of the Raman bands is from both removal of oxo W=O and coordination of olefins to the surface WO_x sites that results in band broadening. The absence of detectable Raman bands from the surface WO_x sites after 120 minutes of reaction suggests that 100% of the surface WO_x sites have become activated after extended reaction times. It is not possible to determine the molecular structures of the activated surface WO_x sites during olefin metathesis from the presented data and, in general, is quite difficult to ascertain since multiple surface tungsten oxide structures can possess the same oxidation states (e.g., $W^{+6}O_x$, $W^{+6}{=}CH_2$, $W^{+6}{=}CHCH_3$ and $W^{+6}O_3$ NPs when present).

At higher tungsten oxide loadings, where crystalline WO_3 NPs are also present, the WO_3 NPs also undergo partial reduction during activation with propylene since there is loss of oxygen at lower temperatures when WO_3 NPs are present, as shown by the formation of oxygenated reaction products (see Figures 8 and 10), and selective decrease in the Raman intensity of the WO_3 NPs (see Figure 7). This is especially evident for evolution of H_2O-TPSR at ~485°C that is only formed when WO_3 NPs are present (see Figure 8). This suggests that partially reduced WO_{3-x} NPs are also present during propylene metathesis for high loaded silica-supported tungsten oxide catalysts.

All the supported surface WO_x sites on SiO_2 become activated by exposure to propylene at elevated temperatures (see Figures 7 and 11). The $C_3^=$-TPSR experiments, however, reveal that there are two distinct activated surface WO_x sites after high temperature activation with

propylene since formation of $C_4^=$ occurs at both ~220 and ~600°C. The activated surface WO_x sites associated with the ~220°C reaction, however, are ~10^{11}x more active than the surface WO_x sites responsible for the ~600°C reaction (assuming 1st-order kinetics and application of Redhead equation[43]). This strongly suggests that the surface WO_x sites associated with the ~220°C reaction are the catalytic active sites when propylene metathesis is conducted below 500°C and represents ~5-10% of the total surface WO_x sites on the SiO_2 support depending on WO_x loadings and C_3= partial pressure.

Although the supported WO_3 NPs also become activated by propylene at elevated temperatures, the resulting WO_{3-x} sites are not active for propylene metathesis since their presence does not affect the activity (see Figure 12).

Andreini *et al.* claimed that a high temperature pretreatment in He (inert) both decreases the break-in time and improves the catalytic activity by a factor of 1.5 when the He pretreatment was performed at ~550°C and the reaction was run at ~380 °C.[44] However, Luckner *et al.* performed both the He pretreatment and reaction studies at the same temperature of ~423°C and found that although the He treatment decreases the break-in time, the catalytic activity is about the same over a longer period of 650 minutes (~11 hours).[45]This discrepancy could be attributed to the different activation temperatures in both studies and such pretreatment effects on number of catalytic active sites will be discussed in a subsequent communication.

4.3. Surface Reaction Intermediates

Direct information about the nature of the surface reaction intermediates is not available from the characterization measurements performed in this study. The high reaction temperature required for propylene metathesis by supported WO_x/SiO_2 catalysts results in a very low

concentration of surface reaction intermediates that is difficult to detect (*in situ* IR could not observe any reaction intermediates, which was not shown for brevity). This is also indicated by the need to have propylene in the gas phase in order for the metathesis reaction to proceed (see Figure 11).

Olefin metathesis for trans-2-butene and ethylene by crystalline WO_3 slabs was examined with DFT calculations by Cheng *et al.*[46,47] It was concluded that trans-2-butene more readily forms $W{=}CHCH_3$ intermediates than ethylene formation of $W{=}CH_2$ intermediates. Consequently, the $W{=}CHCH_3$ intermediates should propagate the metathesis reaction faster than the $W{=}CH_2$ intermediates and the [2+2] cycloaddition of *trans*-2-butene to form the oxametallacycle ring is the rate-determining step.[46] The use of crystalline WO_3 slabs in this DFT investigation is problematic since the experimental studies have demonstrated that crystalline WO_3 is not able to perform olefin metathesis and that the metathesis reaction occurs on the isolated surface WO_x sites.[6,48] DFT calculations with isolated surface WO_x sites would be more relevant to olefin metathesis by supported WO_x/SiO_2 catalysts and are expected to be reported in the near future.

4.4. Structure-Activity/Selectivity Relationships

The activity of the supported WO_x/SiO_2 catalysts for propylene metathesis is directly related to the concentration of surface WO_x sites as shown by the direct relationship between the increasing reaction rate with increasing amount of surface WO_x sites (see Figures 9 and 12). This structure-activity relationship implicates the surface WO_x sites as the catalytic active sites for propylene metathesis by supported WO_x/SiO_2 catalysts. As indicated above, the nature of the activated surface WO_x sites during propylene metathesis is presently not known. The Lewis acid

character[39] of the surface WO_x sites on SiO_2 is responsible for formation of some byproduct C_4-C_6 alkanes and formation of butane is the most sensitive to the concentration of surface WO_x sites.

It is difficult to determine the relative contributions of the isolated surface dioxo $(O=)_2W(-O)_2$ and mono-oxo $O=W(-O)_4$ sites to propylene metathesis since both sites are always present in the same ratio for the supported <8% WO_x/SiO_2 catalysts and become activated in the olefin environment. It may be argued that the initial surface dioxo $(O=)_2W(-O)_2$ site plays a more important role in olefin metathesis because of its much greater concentration in the initial catalyst since it represents ~92% of the total surface WO_x sites. DFT calculations may be able to provide more insights about the reactivity of the two distinct surface WO_x sites. From DFT calculations of olefin metathesis by supported MoO_x/SiO_2 catalysts, which is the system most similar to supported WO_x/SiO_2, Handzlik concluded that coordinated dioxo pseudo-MoO_4 sites attached to two adjacent silanol groups are the catalytic active sites.[49] Furthermore, the five-coordinated mono-oxo surface MoO_5 site is not active for olefin metathesis because of the high activation barrier involved in both formation of cyclobutane intermediates and cycloreversal steps.[50]

The supported crystalline WO_3 NPs are not active for propylene metathesis as reflected in the lack of increase in reaction rate with increasing amount of crystalline WO_3 NPs (Figure 12). The supported crystalline WO_3 NPs adversely impact the olefin metathesis product selectivity (Figure 13) and their easier activation does not contribute to higher olefin metathesis activity (Figures 6 and 12). The Brønsted acid sites [39-41] present on the crystalline WO_3 NPs dimerize $C_2^=$ to $C_4^=$ as well as forming additional C_4-C_6 alkanes.

The acidic characteristics of the surface WO_x sites and WO_3 NPs on SiO_2 account for the promotion of commercial supported WO_x/SiO_2 propylene metathesis catalysts with basic Na or K to neutralize the catalyst acid sites and minimize undesired dimerization of $C_2^=$ to $C_4^=$ as well as forming the undesired C_4-C_6 alkane products.[48]

There are conflicting reports in literature about the molecular structure-metathesis activity relationships for the supported WO_x/SiO_2 catalyst system. An early study by Thomas *et al.* claimed from Raman spectra collected under ambient conditions, XPS in vacuum and H_2-TPR studies that a high degree of dispersion and an easier reducibility are requirements for activity of both supported WO_x/SiO_2 and MoO_x/SiO_2 catalysts.[6] A more recent study by Hua *et al.* with supported WO_x/MTS-9 (titanium-silica sieve) concluded that WO_4 and WO_6 coordinated polytungstates are the catalytic active sites for metathesis rather than WO_3 NPs.[16] These reactivity findings are in agreement with the present study that the surface WO_x sites are the catalytic active sites for olefin metathesis and that WO_3 NPs don't contribute to olefin metathesis activity. The characterization measurements of the catalysts in the earlier studies, however, were performed under ambient conditions where the catalysts are hydrated and the WO_x structures are not relevant to olefin metathesis reaction conditions. The present study demonstrates that the surface WO_x are present as isolated dioxo $(O=)_2WO_4$ and mono-oxo $O=WO_4$ sites prior to olefin metathesis and become partially reduced during olefin metathesis.

5. Conclusions

The supported WO_x/SiO_2 catalysts consist of isolated surface WO_x sites on silica (dioxo $(O=)_2W(-O)_2$ and mono-oxo $O=WO_4$) and crystalline WO_3 NPs. Although both surface WO_x sites are activated by propylene by removal of oxygen, the dominant surface $(O=)_2W(-O)_2$ is

most likely the catalytic active precursor site. Activation produces a highly active catalytic site that can perform metathesis at modest temperatures (~150-250°C) and represents about ~5-10% of the total surface WO_x sites. The concentration of surface reaction intermediates is very low because of the required elevated metathesis temperatures and, consequently, the reaction only proceeds in the presence of gas phase propylene. The crystalline WO_3 NPs become partially reduced to WO_{3-x} during propylene metathesis, but are not able to perform the metathesis reaction. The Lewis and Brønsted acid character of the surface WO_x sites and WO_3 NPs, respectively, is responsible for the byproducts formed by $C_2^{=}$ dimerization to $C_4^{=}$ and oligomerization to C_4-C_6 alkanes. The present study represents the *first time* that molecular level structure-activity/selectivity relationships have been established for propylene metathesis by conventionally impregnated supported WO_x/SiO_2 catalysts.

Supporting Information

Supporting Information Available: Additional Raman, XANES/EXAFS and TPSR figures (Figure S1-S8). This material is available free of charge via the Internet at http://pubs.acs.org.

Acknowledgements

SL and IEW gratefully acknowledge the financial support by the NSF Grant CHE 1301262. AIF and YL gratefully acknowledge funding of their work by the U. S. DOE Grant No. DE-FG02-03ER15476. We acknowledge the facilities support provided at the National Synchrotron Light Source at the Brookhaven National Laboratory (US Department of Energy, Office of Basic Energy Sciences, Contract No. DE-SC0012704) and the Synchrotron Catalysis

Consortium (US Department of Energy, Office of Basic Energy Sciences, Grant No. DE-SC0012335).

References

1. Mol, J. C. *J. Mol. Catal. A: Chem.* **2004***, 213*, 39–45.
2. Mol, J. C. *Catal. Today* **1999**, *51*, 289–299.
3. van Schalkwyk, C.; Spamer, A.; Moodley, D.J.; Dube, T.; Reynhardt, J.; Botha, J.M.; Vosloo, H.C.M. *Appl. Catal. A: Gen.* **200**3, *255*, 143–152.
4. Spamer, A.; Dube, T.I.; Moodley, D.J.; van Schalkwyk, C.; Botha, J.M. *Appl. Catal. A: Gen.* **2003**, *255*, 133–142.
5. van Roosmalen, A. J.; Mol, J.C. *J. Catal*. **1982**, *78*, 17–23.
6. Thomas, R.; Moulijn, J. A.; De Beer, V. H. J.; Medema, J. *J. Mol. Catal.* **1980**, *8*, 161–174.
7. van Roosmalen, A. J.; Koster, D.; Mol, J. C. *J. Phys. Chem.* **1980**, *84*, 3075–3079.
8. Verpoort, F.; Fiermans, L.; Bossuyt, A. R.; Verdonck, L. *J. Mol. Catal.* **1994**, *90*, 43–52.
9. Verpoort, F.; Bossuyt, A.; Verdonck, L. *Chem. Comm*. **1996**, *3*, 417-418.
10. Verpoort, F.; Bossuyt, A. R.; Verdonck, L. *J. Elect. Spect. Related Phenom*. **1996**, *82*, 151–163.
11. Basrur, A. G.; Patwardhan, S. R.; Vyas, S. N. *J. Catal*. **1991**, *127*, 86–95.
12. Martín, C.; Malet, P.; Solana, G.; Rives, V. *J. Phys. Chem. B* **1998**, *102*, 2759–2768.
13. Davazoglou, D.; Moutsakis, A.; Valamontes, V.; Psycharis, V.; Tsamakis, D. *J. Electro. Soc.* **1997**, *144*, 595–599.
14. Wang, Y.; Chena, Q.; Yang, W.; Xie, Z.; Xua, W.; Huang, D. *App. Catal. A: Gen*. **2003**, *250*, 25–37.

15. Hua, D.; Chen, S.; Yuan, G.; Wang, Y.; Zhang, L. *Trans. Metal Chem.* **2011**, *36*, 245–248.

16. Hua, D.; Chen, S.; Yuan, G.; Wang, Y.; Zhao, Q.; Wang, X.; Fu, B. *Micro. Meso. Mat.* **2011**, *143*, 320–325.

17. Chaemchuen, S.; Phatanasri, S.; Verpoort, F.; Sae-ma, N.; Suriye, K. *Kinet. Catal*. **2012**, *53*, 247–252.

18. Liu, N.; Ding, S.; Cui, Y.; Xue, N.; Luming Peng, L.; Guo, X.; Ding, W. *Chem. Eng. Res. Des.* **2013**, *91*, 573–580.

19. Huang, S.; Liu, S.; Zhu, Q.; Zhu, X.; Xin, W.; Liu, H.; Feng, Z.; Li, C.; Xie, S.; Wang, Q.; Xu, L. *App. Catal., A: Gen*. **2007**, *323*, 94–103.

20. Ross-Medgaarden, E.I.; Wachs, I.E. *J. Phys. Chem. C* **2007**, *111*, 15089–15099.

21. Ostromecki, M.M.; Burcham, L.J.; Wachs, I.E.; Ramani, N.; Ekerdt, J.G. *J. Mol. Catal. A: Chem.* **1998**, *132*, 43–57.

22. Lee, E. L.; Wachs, I. E. *J. Phys. Chem. C* **2007**, *111*, 14410 – 14425.

23. Kim, D.S.; Ostromecki, M.; Wachs, I.E. *J. Mol. Catal. A: Chem*. **1996**, *106*, 93–102.

24. Hamieh, A.; Chen, Y.; Abdel-Azeim, S.; Abou-hamad, E.; Goh, S. ; Samantaray, M.; Dey, R.; Cavallo, L.; Baaset, J. M. *ACS Catal* **2015**, *4*, 2164–2171.

25. Mougel, V.; Pucino, M.; Coperet, C. *Organometallics* **2015**, *34*, 551–554.

26. Conley, M. P.; Mougel, V.; Peryshov, D. V.; Forrest, W. P., Jr.; Gajan, D.; Lesage, A.; Emsley, L.; Coperet, C.; Schrock, R. R. *J. Am. Chem. Soc*. **2013**, *135*, 19068−19070.

27. Bouhoute, Y.; Garron, A.; Grekov, G.; Szeto, K. C.; Mallmann, A. D.; Rosal, I. D.; Maron, L.; Girard, G.; Gauvin, R. M.; Delevoye, L.; Taoufik, M. *ACS Catal* **2014**, *4*, 4232–4241.

28. Mazoyer, E.; Merle, N.; Mallmann, A. D.; Basset, J.; Berrier, E.; Delevoye, L.; Paul, J.; Nicholas, C. P.; Gauvin, R. M.; Taoufik, M. *Chem. Comm.* **2010**, *46*, 8944–8946.

29. Bouhoute, Y.; Grekov, D.; Szeto, K. C.; Merle, N.; Mallmann, A. D; Lefebvre, F.; Raffa, G.; Rosal, I. D.; Maron, L.; Gauvin, R. M.; Delevoye, L.; Taoufik, M. *ACS Catal* **2016**, *6*, 1–18.

30. Tian, H.; Roberts, C.A.; Wachs, I.E. *J. Phys. Chem. C* **2010**, *114*, 14110–14120.

31. Stobie, K. M.; Bell, Z. R.; Munhoven, T. W.; Maher, J. P.; McCleverty, J. A.; Ward, M. D.; McInnes, R. J. L.; Totti, F. Gatteschi. *Dalton Trans*. **2003**, 36–45.

32. Seo, J. PhD Dissertation. Brown University. **2013**.

33. Grunert, W.; Morke, W.; Feldhaus, R.; Anders, K. *J. Catal*. **1989**, *117*, 485–494.

34. Yoshinaga, Y.; Kudo, M.; Hasegawa, S.; Okuhara, T. *Appl. Surf. Sci*. **1997**, *121/122*, 485–494.

35. Horsley, J. A.; Wachs, I. E.; Brown, J. M.; Via, G. H.; Hardcastle, F. D. *J. Phys. Chem.* **1987**, *91*, 4014–4020.

36. Balerna, A.; Bernieri, E.; Burattini, E.; Kuz'min, A.; Lusis, A.; Purans, J.; Cikmacs, P., *Nucl. Instrum. Methods Phys. Res., Sect. A* **1991**, *308*, 240–242.

37. Burcham, L. J.; Wachs, I. E. *Spectrochim. Acta* **1998**, *54*, 1355–1368.

38. Chan, S. S.; Wachs, I. E.; Murrell, L. L. *J. Catal*. **1984**, *90*, 150–155.

39. Macht, J.; Iglesia, E. *Phys. Chem. Chem. Phys.* **2008**, *10*, 5331–5343.

40. Yang, X.; Dai, W.; Gao, R.; Fan, K. *J. Catal.* **2007**, *249*, 278–288.

41. Ross-Medgaarden, E. I.; Knowles, W. V.; Kim, T.; Wong, M. S.; Zhou, W.; Kiely, C. J.; Wachs, I. E. *J. Catal*. **2008**, *256*, 108–125.

42. Amakawa, K.; Sun, L.; Guo, C.; Havecker, M.; Kube, P.; Wachs, I. E.; Lwin, S.; Frenkel, A. I.; Patlolla, A.; Hermann, K.; Schlogl, R.; Trunschke, A. *Angew. Chem., Int. Ed*. **2013**, *52*, 13553−13557.

43. Redhead, P.A. Vacuum 1962, 12, 203–211.

44. Andreini, A.; Mol, J. C. *J. Colloid Interface Sci*. **1981**, *84*, 57–65.

45. Luckner, R. C.; Wills, G. B. *J. Catal*. **1973**, *28*, 83–91.

46. Cheng, Z.; Lo, C. *ACS Catal*. **2012**, *2*, 341−349.

47. Cheng, Z.; Lo, C. *ACS Catal*. **2015**, *5*, 59−72.

48. Spamer, A.; Dube, T. I.; Moodley, D. J.; van Schalkwyk, C.; Botha, J. M. *App. Catal. A. Gen.* **2003**, *255*, 153–167.

49. Handzlik, J. *J. Phys. Chem. B* **2005**, *109*, 20794–20804.

50. Handzlik, J. *J. Phys. Chem. C* **2007**, 111, 9337–9348.

TOC: